

LM-04K163  
January 26, 2005

---

---

## Quaternary InGaAsSb Thermophotovoltaic Diode Technology

M Dashiell, J Beausang, H Ehsani, G Nichols, D Depoy, L Danielson, P Talamo, K  
Rahner E Brown, S Burger, P Fourspring, W Topper, P Baldasaro, C Wang, R  
Huang, M Connors, G Turner, Z Shellenbarger, G Taylor Jizhong Li, R Martinelli, D  
Donetski, S Anikeev, G Belenky and S Luryi

---

---

### NOTICE

This report was prepared as an account of work sponsored by the United States Government. Neither the United States, nor the United States Department of Energy, nor any of their employees, nor any of their contractors, subcontractors, or their employees, makes any warranty, express or implied, or assumes any legal liability or responsibility for the accuracy, completeness or usefulness of any information, apparatus, product or process disclosed, or represents that its use would not infringe privately owned rights.

# Quaternary InGaAsSb Thermophotovoltaic Diode Technology

M.W. Dashiell, J.F. Beausang, H. Ehsani, G.J. Nichols, D.M. Depoy, L.R. Danielson, P. Talamo, K.D. Rahner, E.J. Brown, S.R. Burger, P.M. Fourspring, W.F. Topper, P.F. Baldasaro,  
*Lockheed Martin Corporation, Schenectady, New York 12301-1072*

C.A. Wang, R. Huang, M. Connors, G. Turner,  
*MIT Lincoln Laboratory, Lexington Massachusetts 02420-9108*

Z. Shellenbarger, G. Taylor, Jizhong Li, R. Martinelli,  
*Sarnoff Corporation, Princeton, New Jersey 08543-5300*

D. Donetski, S. Anikeev, G. Belenky and S. Luryi  
*State University of New York, Stony Brook, New York 11794-2350*

## Abstract.

Thermophotovoltaic (TPV) diodes fabricated from InGaAsSb alloys lattice-matched to GaSb substrates are grown by Metal Organic Vapor Phase Epitaxy (MOVPE). 0.53eV InGaAsSb TPV diodes utilizing front-surface spectral control filters have been tested in a vacuum cavity and a TPV thermal-to-electric conversion efficiency ( $\eta_{\text{TPV}}$ ) and a power density (PD) of  $\eta_{\text{TPV}}=19\%$  and  $\text{PD}=0.58 \text{ W/cm}^2$  were measured for  $T_{\text{radiator}}=950 \text{ }^\circ\text{C}$  and  $T_{\text{diode}}=27 \text{ }^\circ\text{C}$ . Recombination coefficients deduced from minority carrier measurements and the theory reviewed in this article predict a practical limit to the maximum achievable conversion efficiency and power density for 0.53eV InGaAsSb TPV. The limits for the above operating temperatures are projected to be  $\eta_{\text{TPV}}=26\%$  and  $\text{PD}=0.75 \text{ W/cm}^2$ . These limits are extended to  $\eta_{\text{TPV}}=30\%$  and  $\text{PD}=0.85 \text{ W/cm}^2$  if the diode active region is bounded by a reflective back surface to enable photon recycling and a two-pass optical path length. The internal quantum efficiency of the InGaAsSb TPV diode is close to the theoretically predicted limits, with the exception of short wavelength absorption in GaSb contact layers. Experiments show that the open circuit voltage of the 0.53eV InGaAsSb TPV diodes is not strongly dependent on the device architectures studied in this work where both N/P and P/N double heterostructure diodes have been grown with various acceptor and donor doping levels, having GaSb and AlGaAsSb confinement, and also partial back surface reflectors. Lattice matched InGaAsSb TPV diodes were fabricated with bandgaps ranging from 0.6 to 0.5eV without significant degradation of the open circuit voltage factor, quantum efficiency, or fill factor as the composition approached the miscibility gap. The key diode performance parameter which is limiting efficiency and power density below the theoretical limits in InGaAsSb TPV devices is the open circuit voltage. The open circuit voltages of state-of-the-art 0.53eV InGaAsSb TPV diode are  $\sim 10\%$  lower than the predicted semi-empirical limit to open circuit voltage for a device having absorbing substrate; the voltages are  $\sim 17\%$  below that for an Auger-limited device having back surface reflector and two-pass optical design.

## 1.0 Introduction

Thermophotovoltaic (TPV) converters have attracted interest in the field of direct energy conversion due to the potential for efficient electric generation. For TPV hot side temperatures of approximately 1000-1500°C, achieving greater than 20% thermal to electric efficiency requires: (i) spectral control which recuperates the large portion of below bandgap photons and transmits the above-bandgap photons to the TPV diode [1-3] and (ii) efficient photovoltaic conversion of the above bandgap photons to electric power. The highest reported thermal to electric TPV efficiencies for in-vacuum tests at  $T_{\text{radiator}} \approx 950$  °C and  $T_{\text{diode}} \approx 27$  °C, are 22% for 0.6eV InGaAs/InP[4] and 19% for 0.53eV InGaAsSb/GaSb systems [3]. The 4cm<sup>2</sup> TPV diode/modules in references [3,4] utilized a front surface plasma/interference spectral control filter [5-6]. The 0.6 eV InGaAs TPV diodes which demonstrated the record conversion efficiency were grown using step graded InPAs buffer layers to accommodate the lattice mismatch between the InGaAs active region and the InP substrate. The InGaAsSb material system was investigated because it can be grown lattice-matched to GaSb substrates for bandgaps as low as 0.5eV [7-11]. Low bandgap TPV diodes are of interest because of the greater power density and better spectral performance associated with the smaller energy gap [1-3].

This article presents modeling predictions and experimental data detailing the influence of diode architecture for 0.53eV InGaAsSb TPV diodes grown by Metal Organic Vapor Phase Epitaxy (MOVPE) on GaSb substrates having double heterostructure confinement. Standard expressions and numerical solutions for the semiconductor transport equations are used to predict TPV diode performance. The recombination coefficients of 0.53eV InGaAsSb material have been estimated from minority carrier lifetime measurements and are input as parameters in the simulations. These simulations determine a semi-empirical efficiency and power density limit for the conversion of thermal-radiation to electric power. Measured efficiency and power density indicate the 0.53eV InGaAsSb TPV diode is well below the semi-empirical limit, primarily because the open circuit voltage is limited by parasitic recombination which might be related to intrinsic defects of the antimonide materials. Additional parasitics limiting the efficiency include parasitic absorption in the front surface filter and GaSb contact layer. The following sections discuss: TPV efficiency (section 2) 0.53eV InGaAsSb TPV modeling assumptions (section 3), the intrinsic limits imposed by Auger recombination (section 4), the simulation and theoretical results (section 5), the experimental diode electrical/optical results (section 6), bandgapdependence of dark current and quantum efficiency (section 7), measured

in-cavity TPV efficiency (section 8), and a discussion of results (section 9). An appendix is included which gives detailed TPV diode and spectral assumptions.

## 2.0 Thermophotovoltaic Efficiency ( $\eta_{TPV}$ )

In this article the TPV thermal-to-electric conversion efficiency  $\eta_{TPV}$  is defined as the maximum electrical power output from the TPV diode/module divided by the total thermal power absorbed in the diode. In the work presented here TPV efficiency is modeled and measured with a vacuum gap separating the TPV diode module from the radiator thus the heat absorbed in the diode is due to radiative heat transfer only. Because of the very large fraction of the unusable below bandgap photons, it is convenient to evaluate the overall TPV efficiency in terms of the diode efficiency  $\eta_{Diode}$  and the spectral efficiency  $\eta_{Spectral}$  [1,3]. The former term characterizes the efficiency of converting above bandgap photons absorbed in the diode into electricity. The latter term,  $\eta_{Spectral}$ , quantifies the ratio of above bandgap photon power absorbed by the diode over the total radiative power absorbed in the diode. The maximum power from the TPV diode/module under illumination is the product of the open circuit voltage ( $V_{OC}$ ), the short circuit current ( $I_{SC}$ ), and the fill factor (FF) [12]. For a TPV cavity having an effective emissivity  $\epsilon_{eff}$ , above bandgap diode reflectivity  $R$ , parasitic absorbance  $\alpha_{parasitic}$  (e.g. absorbance in the front surface filter), and diode area ( $A$ ), the diode efficiency and spectral efficiency can be generally written as:

$$\eta_{Diode} = \frac{V_{OC} \times I_{SC} \times FF}{A \int_{E_{Gap}}^{\infty} \epsilon_{eff} (1 - \alpha_{parasitic}) \frac{2\pi E^3}{h^3 c^2 (e^{E/kT_{Radiator}} - 1)} dE} \quad (1)$$

$$\eta_{Spectral} = \frac{A \int_{E_G}^{\infty} \epsilon_{eff} (1 - \alpha_{parasitic} - R) \frac{2\pi E^3}{h^3 c^2 (e^{E/kT_{Radiator}} - 1)} dE}{A \int_0^{\infty} \epsilon_{eff} \frac{2\pi E^3}{h^3 c^2 (e^{E/kT_{Radiator}} - 1)} dE} \quad (2)$$

$$\eta_{TPV} = \eta_{Spectral} \times \eta_{Diode} = \frac{V_{OC} \times I_{SC} \times FF}{A \int_0^{\infty} \epsilon_{eff} \frac{2\pi E^3}{h^3 c^2 (e^{E/kT_{Radiator}} - 1)} dE} \quad (3)$$

Where  $E$ ,  $h$ ,  $k$ ,  $c$  and  $T_{radiator}$  are photon energy, Planck's constant, Boltzmann's constant, the speed of light and the radiator (hot side) temperature. The above calculations the effective emissivity takes into account the spatial and energy dependence of the module's reflectivity and emissivity. This level of

detail and the assumptions made in spectral efficiency calculations for the predictions in this article are given in Table A1 of the appendix..

The thermodynamic limit to photovoltaic conversion efficiency is determined from fundamental radiative processes and the intrinsic radiative currents between the hot radiator and cold diode and was originally described by Shockley and Queisser for single bandgap diodes [13] and expanded to more general photovoltaic devices such as tandem solar cells [14] and thermophotovoltaics [1]. The thermodynamic limit to single bandgap TPV efficiency can be represented with a diode architecture having: (i) perfect below-bandgap photon recuperation (ii) carrier generation/recombination in the TPV diode occurring only via radiative processes (iii) the device has a perfectly reflecting back surface which limits the escape of recombination radiation to the front surface only, and (iv) no parasitic (i.e. free carrier) absorption at the cold side. For 0.53eV TPV the thermodynamic limit for  $T_{\text{Radiator}}=1000^{\circ}\text{C}$  and  $T_{\text{Diode}}=27^{\circ}\text{C}$  is  $\eta_{\text{TPV}}(0.53\text{eV}) = 45\%$  [1].

While the thermodynamic limit provides a theoretically based maximum limit to TPV conversion efficiency, real TPV diodes will have further energy losses and entropy sources beyond the radiative limit which must be quantified both with experimental data and mathematical models. This article uses established semiconductor theory and empirically determined values of InGaAsSb material coefficients [15-17] and TPV front surface spectral control filters parameters [5-6] to provide a practical engineering limit to TPV conversion efficiency for the 0.53eV InGaAsSb TPV material system. We refer to this practical limit for 0.53eV InGaAsSb TPV as the semi-empirical limit, originally named in reference [13] to distinguish predictions based on empirically determined material constants from material-independent thermodynamic analyses.

### **3.0 0.53eV InGaAsSb TPV modeling assumptions**

In this work we used the spectral control characteristics that are achieved using front surface filters with properties similar to those measured in state of the art TPV filters[5-6] However for ease of calculations we assumed a step-function profile for the semi-empirical limits. The Appendix provides the specific details and numerical values used for spectral efficiency calculations.

#### **3.1 Spectral Control**

From angle and wavelength dependent transmission and reflection measurements of front surface TPV spectral control filters (tandem interference and plasma filters), spectral efficiencies of

$\eta_{\text{Spectral}} \sim 80\%$  and above bandgap transmission of 79% have been demonstrated for  $T_{\text{Radiator}} = 950^\circ\text{C}$  and cutoff wavelengths of  $\sim 0.53\text{eV}$  [1,5-6]. For simplicity, the efficiency calculations in this article assume a simplified step function spectral reflection profile where the filter reflects 97% of below bandgap photons, 15% of above bandgap photons and has a  $\sim 2\%$  parasitic absorbance of above bandgap photons. Table A1 of the appendix details the spectral efficiency calculations, where the step function approximation gives a value of  $\eta_{\text{Spectral}}(E_G \sim 0.53\text{eV}, T_{\text{Radiator}} = 950^\circ\text{C}) = 87\%$ . This value estimates a semi-empirical limit to 0.53eV TPV spectral efficiency based on the materials and designs currently used in state-of-the-art front surface filters.

### 3.2 TPV Diode Assumptions

Simulation of the photovoltaic conversion of above bandgap energy (Equation 1) was performed using PC-1D, a numerical photovoltaic simulator which solves the steady state carrier transport equations for electrons and holes, Poisson's equation, and carrier continuity equations. The diode architectures considered are shown in Figure 1. Electron-hole generation rates were computed from the radiation power spectrum and absorption coefficient of the 0.53eV InGaAsSb material. The net recombination rates ( $R_i$ ) in the diode are modeled using the standard equations listed below (eqns. 4-7). The net radiative recombination rate, will differ from the value calculated via the radiative recombination rate predicted from the Shockley van Roosbroek (SvR) detailed-balance model [18], because of photon recycling in the active region. The photon recycling resulting from photons produced from electron-hole pair recombination is a function of the optical boundary conditions and thickness of the diode and the net radiative recombination coefficient must be corrected by a photon recycling factor  $\phi$  [19,20]. The net radiative recombination rate used in the simulation, after correcting for photon recycling, effects is given by equation (4)

$$R_{\text{Rad}} = \frac{B}{\phi} (np - n_i^2) \quad (4)$$

Where B is the radiative recombination coefficient calculated via SvR relation and  $\phi$  (in the absence of free carrier absorption) is the inverse ratio of the sum of the photon flux exiting the diode's front and back surfaces to the total number of radiative recombination events occurring within the diode volume. The photon recycling factor must be calculated outside of the numerical simulator for the diode architecture under investigation-using the equations given in Table A2. The quantities n and p in

equation (4) are the electron and hole carrier densities under illumination and  $n_i$  is the intrinsic carrier density.

The net Auger recombination rate is given by equation (5)

$$R_{Aug} = (C_n n + C_p p)(np - n_i^2) \quad (5)$$

and the Shockley Read Hall (SRH) and surface/interface recombination (SRV) rates are modeled by equations (6) and (7) respectively

$$R_{SRH} = \frac{(np - n_i^2)}{\tau_n (p + n_i e^{-E_i/kT}) + \tau_p (n + n_i e^{-E_i/kT})} \quad (6)$$

$$R_{SRV} = \frac{S_n S_p (np - n_i^2)}{S_n (p + n_i e^{-E_i/kT}) + S_p (n + n_i e^{-E_i/kT})} \quad (7)$$

where the material recombination coefficients  $\tau_{n,p}$  (Shockley Read Hall lifetime for electrons and holes),  $S_{n,p}$  (surface/interface recombination velocity), and  $C_{n,p}$  (Auger recombination coefficients) were parametrically varied in the simulations about the values reported in minority carrier lifetime studies of the p-type 0.53eV InGaAsSb materials[15-17]. SRH and SRV recombination are assumed to occur through deep levels defects with energies centered near mid-gap. Unless otherwise stated we assumed the recombination coefficients were equivalent for the p-type and n-type InGaAsSb.

#### 4.0 Intrinsic Auger limitations to TPV diode efficiency

As discussed in the introduction, radiative recombination/generation represents the minimum loss (or entropy generation) in photovoltaics because of the principle of detailed balance between generation and recombination of carriers required to maintain thermal equilibrium with the background photon population at  $T_{cold}$ . Semiconductor photovoltaic diodes will have additional contributions to the thermal generation/recombination rates due to non-radiative processes (e.g. impact ionization/Auger recombination). The total thermal equilibrium carrier generation/recombination rates determine the diode dark current which is used to mathematically describe the current-voltage relationship of a photovoltaic diode[1,12-14]. The standard mathematical model shows that the open circuit voltage  $V_{OC}$ , and thus  $\eta_{Diode}$ , are proportional to the logarithm of the ratio of light generated current to the dark current:  $V_{OC} = \frac{kT}{q} \ln\left(\frac{I_{light}}{I_o}\right)$ . The diode parameters, FF and  $I_{SC}$ , in the numerator of equation (1) are

determined primarily by optical design and minimization of parasitic resistance (note that theoretically, the fill factor also depends on dark current [1] for negligible parasitic resistances) .

The minimum radiative component of the dark current is achievable with a back surface reflector (BSR) in place of a partially absorbing substrate/back contact that is often used in photovoltaic devices. The BSR eliminates the large density of photon modes, that would be available in a high index semiconductor substrate (i.e. the  $n_{\text{refractive}}^2$  factor is eliminated in the radiative dark current expression for devices having perfect BSR) [1]. In real photovoltaic diodes non-radiative recombination are additive losses which degrade device efficiency, primarily by increasing the diode's dark current above its radiatively limited value. If the non-radiative losses become so severe that the electron and hole diffusion lengths becomes small compared to the active region thickness, the quantum efficiency will also degrade.

In concept, non-radiative recombination due to Shockley Read Hall defects might be eliminated via improving material quality; however, Auger recombination/generation is a fundamental process which cannot be eliminated by design or by material improvements other than reducing the layer thickness of the absorbing active region and reducing background carrier densities in highly doped active regions [21]. The calculations performed in this work, using empirically determined values of the material recombination coefficients, predict that the Auger recombination will set the maximum obtainable limit to  $V_{OC}$  and  $\eta_{Diode}$  in 0.53eV InGaAsSb TPV. The high injection Auger recombination rate is the minimum Auger recombination rate possible and is determined by the steady state electron-hole population under illumination, (not the background carrier density).

Using the same methodology developed by Green et al. [21] for silicon photovoltaics, we can predict minimum values of the interface recombination velocity and SRH lifetime required to approach the intrinsic Auger limited open circuit voltage assuming a simple geometry. The authors of reference [21], used the expressions given equations (4-7) to solve the Poisson and continuity equation for the open circuit voltage as a function of light generated current density  $J_{\text{Light}}$  for a thick absorbing region of doping  $N_B$  and thickness  $W$ . The SRH lifetime in p-type absorbers should be greater than the values specified by equations 8 and 9, so that SRH recombination does not reduce the diode's open circuit voltage below the Auger limited value.  $\Delta n$  is the steady-state excess carrier density under illumination, and  $C_p$  and  $C_n$  are Auger coefficients in p-type and n-type material. Equation (8) states that the low injection SRH lifetime must be greater than the low injection Auger carrier lifetime in p-type material. By removing doping, the Auger recombination lifetime increases until the illuminated



diode reaches high-injection and the SRH lifetime must be greater than the quantity given in equation (9) in order to achieve the intrinsic Auger limited open circuit voltage. Equation (9) represents the optimal condition.

$$\tau_{SRH}^{low-injection} \gg \frac{1}{C_p N_B^2} \quad \text{for } \Delta n \ll N_B \quad (8)$$

$$\tau_{SRH}^{high-injection} \gg \left[ \frac{q^2 W^2}{J_{Light}^2 (C_p + C_n)} \right]^{1/3} \quad \text{for } \Delta n \gg N_B \quad (9)$$

For TPV current densities of approximately  $J_{Light}=3A/cm^2$  the SRH lifetime should be greater than  $\tau_{SRH} > 1\mu s$  to approach the intrinsic Auger limit when assuming  $C_{n,p} \approx 1 \times 10^{-28} cm^6/s$ . Using the same approach again from [21] the SRV needs to be  $\sim 100 cm/s$  or less. Similar calculations solving for equations 5 and 6 indicate that the photon recycling factor must be  $\phi \gg 5$  under steady state illumination ( $J_{light} \sim 3A/cm^2$ ), to achieve the Auger limited open circuit voltage. This means the InGaAsSb TPV diode requires a back surface reflector to limit the radiative dark current (see Table A2). Minority carrier lifetimes in **p-type** InGaAsSb estimate the SRH lifetime to be in the range of ( $0.5\mu s < \tau_{SRH} \leq 1.1 \mu s$ ) and values of SRV  $\sim 10^2-10^3 cm/s$  [15-17]. Preliminary investigations of the minority carrier lifetime in **n-type** InGaAsSb indicate the SRV at the AlGaAsSb/InGaAsSb and GaSb/InGaAsSb interfaces are less than a few  $\sim 10^3 cm/s$ , however there is evidence of greater SRH activity in n-type InGaAsSb because of a strong excitation dependence of the measured low-injection carrier lifetime in n-type InGaAsSb.. A precise estimate for the SRH lifetime for the relevant light injection levels in n-type InGaAsSb (Te-doped) does not exist, however the preliminary results set a lower bound at  $\tau_{SRH} \geq 0.1\mu s$ .

## 5.0 Numerical simulations of 0.53eV InGaAsSb TPV efficiency

Since intrinsic Auger recombination sets a practical efficiency limit for high quality crystalline material, the importance of determining the Auger coefficients used in equation (5) is of great importance for modeling predictions. Figure 2a and 2b shows predicted efficiency and power density limits as a function of Auger coefficient  $C_{n,p}$  for 0.53eV InGaAsSb diodes having a back surface reflector, negligible defect/interface recombination and the spectral control values given in Table A1 (solid symbols). The authors of reference [15] obtained an Auger coefficient of  $2 \times 10^{-28} cm^6/s$  with an approximate uncertainty of  $\pm 1 \times 10^{-28} cm^6/s$  for p-doped 0.53eV InGaAsSb. Previous literature [7]

revealed that there is a significant scatter among the published reports for Auger coefficients in low bandgap III-V semiconductors. The predicted efficiency and power densities are also plotted for 0.53eV InGaAsSb diode temperatures of 27 °C, 50°C and 100 °C. Upon raising the diode temperatures from 27°C to 100°C the efficiency limit drops from 30% to ~20%, with a corresponding decrease in power density when the Auger coefficient is assumed  $\sim 10^{28} \text{cm}^6/\text{s}$ . A strong temperature dependence is due to the increase of  $n_i^2$ , the intrinsic carrier density. These diode temperatures were chosen because they illustrate the strong temperature effect on TPV diode performance and may give more appropriate semi-empirical performance limits for systems constrained to operate at higher cold-side temperatures. The open-symbols of figure 2a and 2b also shows the predicted efficiency and power density for 0.53eV InGaAsSb TPV diodes having non-negligible bulk and surface recombination for emitter and base regions of the diode, illustrating the stringent material requirements necessary to approach the intrinsic Auger limited performance. The decrease of efficiency and power density predicted for increasing values of Auger coefficients, increasing diode temperatures, and increased defect recombination is primarily due to reduction of diode open circuit voltage.

Open circuit voltage can depend on the device architecture. Figure 3a and 3b shows the parametric studies of the 0.53eV InGaAsSb diode open-circuit voltage as a function of P-type acceptor doping ( $N_A$ ) for varying SRVs for radiator temperatures of 950°C ( $J_{\text{light}} \sim 3 \text{A}/\text{cm}^2$ ). Figure 3a shows the simulations for an 0.53eV InGaAsSb architecture having a back surface reflector. In high-level injection ( $N_A \leq 5 \times 10^{16} \text{cm}^{-3}$ ) the intrinsic Auger recombination rate limits the  $V_{\text{OC}}$  to 370 mV. However, as the SRV increases beyond a few 100 cm/s,  $V_{\text{OC}}$  decreases and becomes interface limited for low-to-moderate dopings. At dopings  $N_A > 5 \times 10^{17} \text{cm}^{-3}$ , the  $V_{\text{OC}}$  is limited by the low-injection Auger carrier lifetime. Figure 3b shows the simulated curve for the 0.53eV InGaAsSb diode architecture having an absorbing back surface. Because of the absorbing substrate/back contact of refractive index ( $n_{\text{refractive}}$ ), the maximum achievable open-circuit voltage of  $V_{\text{OC}} = 340 \text{mV}$  is below the intrinsic Auger limit due to the greater than order of magnitude increase of radiative dark current. A second effect which lowers the predicted open circuit voltage limit of devices with absorbing back substrates is the 2X increase of diode thickness required to account for the reduction of the two-pass to a one-pass optical path length.

The same trends shown in Figure 3a and 3b are observed when the SRH lifetime is parameterized (not shown), and again gives good agreement with the previous analysis stating that the SRH lifetime need be greater than  $\tau_{\text{SRH}} > 1 \mu\text{s}$  to approach the intrinsic Auger limit. Maximum

measured open circuit voltage of 0.53eV InGaAsSb TPV diodes at room temperature to date is about 320mV at current density of 2-3A/cm<sup>2</sup> both with absorbing substrate and with an hybrid back surface reflector [21].

For the TPV parameter range discussed here, the simulated quantum efficiency peaked at ~100% was nearly independent of SRV and SRH-lifetime values investigated in the simulations, however at doping levels approaching 10<sup>19</sup>cm<sup>-3</sup>, where Auger recombination is expected to reduce the diffusion length below the layer thickness, the predicted quantum efficiency (thus short circuit current) is observed to degrade. Quantum efficiency is also predicted to degraded when surface recombination velocities greater than 10<sup>4</sup>cm/s and SRH lifetimes less than 0.1μs are simulated. However considering the TPV device performance discussed in the next sections, the measured values of interface recombination velocity and carrier lifetimes [15-17], we believe the parameter range considered in this article are appropriate; thus V<sub>OC</sub> is the primary diode parameter of equation (1) which is most sensitive to the values of the material recombination coefficients.

Figure 3 illustrates that to obtain the semi-empirical efficiency and power density limits shown in Figure 2, that the 0.53eV InGaAsSb TPV diode requires a back surface reflector and low values of interface recombination velocity (<<500cm/s) and long Shockley Read Hall lifetimes >1μs to approach the intrinsic Auger limited open circuit voltage. However, even with nearly perfect material quality, the high-injection Auger recombination rate limits the open circuit voltage to 0.37 Volts in comparison to ~0.430 Volts which is the absolute thermodynamic limited open circuit voltage [1].

## **6.0 0.53eV InGaAsSb TPV Diode Electrical/Optical Characteristics**

Various 0.53eV InGaAsSb double heterostructure TPV diode architectures were grown by MOCVD. TPV diodes with area 1×0.5 cm<sup>2</sup> and 13% front grid shading were fabricated using standard photolithography and metal evaporation. The front surface of the TPV diodes are passivated with either GaSb (E<sub>g</sub> ≈ 0.73eV) or AlGaAsSb (E<sub>g</sub> ≈ 1.0eV) windows. A doped GaSb contact layer was grown subsequent to the window layer to enable ohmic contact formation for the metal contact grid and prevent oxidation of AlGaAsSb layer. Both GaSb and AlGaAsSb back surface fields (BSF) were investigated to confine minority carriers at the rear of the active diode. Diode illuminated current voltage (IV) characteristics and quantum efficiency (QE) were measured at room temperature. The measured reflection for uncoated epitaxial TPV diode layers was approximately 35% in the range of 800nm-2600nm which was used to calculate for the internal quantum efficiency. Temperatures were

controlled during measurement with a thermoelectric cooler, and the IV curves are measured using 4-point measurement technique. Low ( $< 10\text{m}\Omega$ ) series resistance and good fill factors of  $\sim 70\%$  were routinely observed for all P/N and N/P InGaAsSb TPV diodes at current levels of  $\sim 1\text{-}3\text{A}/\text{cm}^2$ . The electrical and optical measurements discussed in section 6 were performed out of cavity with no-front surface filter or anti-reflection coating on the diodes and were illuminated by lamps rather than a blackbody radiator.

### 6.1 Quantum Efficiency Measurements of 0.53eV InGaAsSb TPV diodes.

Figure 4 shows the typical internal quantum efficiency (IQE) for both N/P and P/N architectures measured for InGaAsSb TPV diodes and the simulated fit assuming  $S_{n,p}=1000\text{cm}/\text{s}$ ,  $\tau_{\text{SRH}}\approx 1\mu\text{s}$ . and  $C_{n,p}=10^{28}\text{cm}^6/\text{s}$ . The measured IQE degrades in both architectures at short wavelength due to absorption in GaSb front contact layers, however the IQE is practically the same for either N/P or P/N architectures having the same GaSb cap thickness. The decrease in quantum efficiency is observed only for wavelengths shorter than 1600nm, the bandgapwavelength of GaSb, and was much more pronounced for thicker GaSb window/cap layers. The shape of the IQE can be fit to the parabolic absorption model for 0.53eV InGaAsSb, except for the long wavelength tail observed for IQE  $< 20\%$ .

Although the carrier lifetimes and diffusion lengths are sufficient to achieve unity internal quantum efficiency, the TPV diode requires the surface passivating window layer (AlGaAsSb or GaSb) [8-10] and the GaSb contact layer for ohmic contact formation. Absorption in these inactive layers reduces the internal quantum efficiency below unity. Figure 5 shows the measured internal quantum efficiency for an N/P 0.53eV InGaAsSb TPV diode having GaSb window and contact layer before and after chemically thinning the GaSb contact layer. A thick GaSb contact layer was grown with a thickness between 400 and 600nm and was subsequently thinned via chemical etching of that sample. The IQE at 1000nm wavelength prior to etching was about 50%. After removing approximately 50-70% of the GaSb cap, the IQE at 1000nm increased to 80% which is in agreement with the simulation. The free GaSb surface is simulated with a surface recombination velocity of  $5\times 10^5\text{cm}/\text{s}$  and the absorption coefficient was taken from measured optical data [24]. Figure 5 also shows the simulated curve for the diodes having only a 10nm thick GaSb (not obtainable experimentally via our chemical etching technique) showing the unity IQE predicted from a diode having very thin GaSb window/contact layer.

Figure 6 shows the IQE curves for two N/P 0.53eV InGaAsSb TPV diodes having equivalent GaSb contact layer thicknesses, however one has a thin AlGaAsSb window layer ( $t_{\text{AlGaAsSb-window}} \ll t_{\text{GaSb-contact}}$ ) to passivate the n-type emitter (refer to figure 1) and the other has a thin GaSb window layer. Figure 6 reveals that the presence of the thin AlGaAsSb causes additional IQE degradation below the cutoff wavelength of the GaSb. The degradation can be explained by the high bandgap of the AlGaAsSb layer relative to both the GaSb cap and the InGaAsSb active region, which effectively acts as a barrier to minority carriers generated in the GaSb cap. When using a GaSb window, the IQE is greater because the minority carriers generated in the GaSb cap may either diffuse into the InGaAsSb active layer and be collected as current or recombine at the free front surface. Structures having the AlGaAsSb minority carrier barrier between InGaAsSb active region and GaSb cap will prevent nearly all minority carriers generated in the GaSb cap from diffusing into the active region. The generic band diagrams with AlGaAsSb window and GaSb windows illustrating the barriers for minority carrier diffusion in the vicinity of the n-type emitter are shown in the inset of Figure 6.

## **6.2 Current Voltage measurements of N/P and P/N 0.53eV InGaAsSb TPV diodes having GaSb or AlGaAsSb double-heterojunction confinement**

Figure 7 shows the open-circuit-voltage vs. short-circuit-current density ( $V_{oc}$ - $J_{SC}$ ) relation measured for various illumination intensities of six different 0.53eV InGaAsSb TPV diodes having different architectures (refer to Figure 1 for the general epitaxial layer schematic). All diodes had double heterostructure confinement composed of either lattice-matched AlGaAsSb or GaSb for the (i) front window used to passivate the emitter surface and (ii) back surface field (BSF) to confine carriers within the active diode's volume. The  $V_{oc}$ - $J_{SC}$  of both P/N (thick p-type emitter/thin n-type base) and N/P (thin n-type emitter/thick p-type base) are included. These electrical characteristics are representative of a large number of diodes grown over several year time frame and fill factors for all architectures were measured to be  $FF \approx 70\%$ . The shape of the  $V_{oc}$ - $J_{SC}$  curve reveals the ideality ( $n$ ) and dark current density  $J_0$  ( $A/cm^2$ ). The ideality may vary between  $n=1$  and  $n=2$  with illumination level according to the Shockley drift/diffusion and Shockley-Read-Hall generation/recombination theory[12], However, in general we observe near unity ideality for all diodes. The lowest dark currents were achieved for the 0.53eV P/N InGaAsSb TPV diodes passivated with p-type AlGaAsSb windows for the front surface and N/P devices having either GaSb or AlGaAsSb front surface passivation. The P/N

TPV diode's dark current appears to be insensitive to whether the n-type back surface field (BSF) material is formed by either a GaSb/InGaAsSb or AlGaAsSb/InGaAsSb interface. The lowest measured room temperature dark current is  $J_0=1.5\times 10^{-5}$  A/cm<sup>2</sup> with an ideality of  $n\approx 1$  for diodes with p-type AlGaAsSb window layers; P/N diodes with P-type GaSb window layers show room temperature dark current of  $J_0=2.5\times 10^{-5}$  A/cm<sup>2</sup> with an ideality of near unity. Shallow emitter N/P have recently been enabled by the development of low-temperature annealed shallow contacts to n-type GaSb [23] and the electrical characteristics are also included in Figure 7. Low dark currents of  $J_0=1.5\times 10^{-5}$  A/cm<sup>2</sup> ( $n\approx 1$ ) are also observed for all N/P architectures, and are independent of whether AlGaAsSb or GaSb is used to confine minority carriers on either the p-side or n-side. Only two measurement points were available for the N/P TPV diode having both n-type and p-type GaSb window and BSF, because of sample breakage.

The authors of reference [16] reports lower (by at a factor of  $\sim 3$ ) effective surface recombination velocities in double heterostructure p-type 0.53eV InGaAsSb lifetime samples using p-type AlGaAsSb confinement rather than p-type GaSb. Our dark current measurements comparing p-GaSb and P-AlGaAsSb confinement provide further insight on the results of reference [16]: using P-type AlGaAsSb front surface windows reduces the P/N diode's dark current compared to using P-type GaSb windows; however, p-type AlGaAsSb and p-type GaSb back surface fields both result in same dark currents for N/P diodes. This indicates that p-type AlGaAsSb passivation layer is suppressing minority carrier diffusion to the free surface of the GaSb contact layer, rather than actually reducing the number of defect states at the interface between active region and passivation layer. If the AlGaAsSb actually reduced the effective SRV through a reduction of the number electrically active interface states, than N/P architectures having p-type GaSb back surface field would result in  $\sim 70\%$  increase in dark current observed using p-type GaSb windows in P/N architectures.

Two different simulated  $V_{OC}$ - $J_{SC}$  curves are also shown in figure 7, assuming  $C_{n,p}=10^{-28}$  cm<sup>6</sup>/s,  $\tau_{SRH} = 1$   $\mu$ s, and: (i) An absorbing back surface and front and back SRV's  $\sim 1000$  cm/s, and (ii) a BSR architecture and SRV's = 20 cm/s. The simulated  $V_{OC}$ - $J_{SC}$  curve in case (ii) approaches the high-level injection Auger-limited open-circuit voltage and shows the semi-empirical limit to open circuit voltage (at the thickness considered in this work) as a function of light generated current density. The simulations illustrate the potential gains in diode open circuit voltage which are achievable by improving the optical boundary conditions of the diode (increased photon recycling) and minimizing defect/interface recombination.

### 6.3 Influence of doping on 0.53eV InGaAsSb TPV diode performance

Section 5 discussed that the shape and magnitude of the predicted open circuit voltage curves vs. doping were dependent on the material quality, the front and back surface recombination velocities, and whether a back surface reflector is used. The measured open circuit data presented in this section corresponds to that from both N/P and P/N architectures where the n-type and p-type doping were varied. The measured open circuit voltage (at  $J_{\text{Light}} \sim 2.5 \text{ A/cm}^2$ ), normalized to the diode bandgap vs. acceptor doping in the p-type absorbing region is shown in Figure 8. A similar variation of the donor doping in the thin n-type region is shown in Figure 9. The error bars assume a  $\sim 5 \text{ mV}$  variability in both measured open circuit voltage and determination of bandgap via quantum efficiency measurements. The open circuit voltage was normalized to the bandgap to account for slight variations in diode bandgap observed during the many growth runs performed. Fill factors for all the devices were  $\sim 70\%$  at  $2\text{-}3 \text{ A/cm}^2$  and measured quantum efficiencies were independent of doping. Included also in Figure 8 is the 0.53eV InGaAsSb Hybrid back surface reflector device reported in [22] and the P/N InGaAsSb diode having p-GaSb windows (high SRVs). Several simulated curves are shown in Figure 8 and 9 for 0.53eV InGaAsSb TPV devices having (i) back surface reflector and negligible SRH and SRV recombination (i.e. the semi-empirical intrinsic Auger limit) and (ii) absorbing substrate architectures with various material SRV values and SRH defect recombination lifetimes. The descriptions of simulated curves in the legend of Figure 8 and Figure 9 of low SRV and negligible bulk defect limited material corresponds to  $\tau_{\text{SRH}} > 1 \mu\text{s}$  and  $\text{SRV} < 100 \text{ cm/s}$ , while bulk defect limited and surface limited simulations correspond  $\tau_{\text{SRH}} = 0.5 \mu\text{s}$  and  $\text{SRV} \sim 2000 \text{ cm/s}$ .

Figures 8-9 reveal no significant change in open circuit voltage for n-type and p-type dopings ranging from approximately high  $10^{16} \text{ cm}^{-3}$  to low  $10^{18} \text{ cm}^{-3}$  and no increase when incorporating a back surface reflector into the device architecture. The only observable change in open circuit voltage factor was observed when p-AlGaAsSb was incorporated as front surface window layer instead of p-GaSb shown again in Figure 8. The open circuit voltage factor did not observable increase when reducing doping and the p-type InGaAsSb/AlGaAsSb SRV from  $10^3 \text{ cm/s}$  to  $< 10^2 \text{ cm/s}$ , and incorporating a back surface reflector, which is predicted if defect recombination do not limit the device (see dashed line). The observed independence of  $V_{\text{OC}}$  on these architectural parameters follows the behavior predicted from that of a diode limited by Shockley Read Hall defect recombination or perhaps surface recombination velocity at the n-type interface. A high p-type surface recombination velocity is ruled out because minority carrier lifetime measurements show that values as low of  $100 \text{ cm/s}$  can be

achieved. A direct measurement of minority carrier lifetime in nominally undoped InGaAsSb material provides a lower bound of  $\tau_{\text{SRH}}(\text{p-type}) > 500\text{ns}$  for the active region of 0.53eV InGaAsSb diodes; extrapolation to zero carrier concentrations indicate that the minority electron  $\tau_{\text{SRH}}$  lifetime is 1300ns in bulk p-InGaAsSb [15]. Preliminary results for n-type InGaAsSb have provided asymptotic limits for defect recombination lifetimes in n-type InGaAsSb: a minimal value of  $\tau_{\text{SRH}}(\text{n-type}) > 100\text{ns}$  and a maximum SRV of about  $10^3\text{cm/s}$  have been determined via the direct measurement of carrier lifetime. Unlike p-type InGaAsSb, the minority carrier lifetime in n-type InGaAsSb samples exhibit a strong dependence on excitation power of their low-injection lifetime, indicating Shockley Read Hall defect activity. 0.53eV TPV diodes having material recombination coefficients near these n-type asymptotes are predicted to be limited by SRH recombination in the bulk and n-type interface in agreement with simulations shown in Figures 8 and 9.

Figures 8 and 9 show that the measured open circuit voltage for both n-type and p-type dopings above  $10^{18}\text{cm}^{-3}$  are greater than the limits predicted by low-injection Auger lifetime and that the open circuit voltage does not degrade at high doping levels. This suggest that the current 0.53eV InGaAsSb TPV diode is not limited by Auger recombination. Further evaluation of Auger recombination in InGaAsSb TPV material is warranted since the deviation at high dopings suggest either the model used in equation (5) or the coefficient values in [15] do not completely describe the recombination processes in InGaAsSb or the model is not valid at high doping levels.

## 7.0 0.5-0.6eV InGaAsSb TPV diodes lattice matched to GaSb

Flexibility in TPV diode band gap, while maintaining lattice matching is an important consideration when choosing a TPV material because the optimal diode bandgap depends on both  $T_{\text{Diode}}$  and  $T_{\text{radiator}}$ . Reference [9] reported high quantum efficiency InGaAsSb TPV diodes having bandgaps ranging from 0.54eV to 0.49eV, however that report showed decrease in open circuit voltage and fill factor as the bandgap was reduced from 0.54eV to 0.49eV (the fill factor decreased from FF=66% to 58% and open circuit voltage factor ( $V_{\text{OC}}/E_{\text{gap}}$ ) from 57% to 48% in reference [9]). In this section we present 0.5eV, 0.53eV, and 0.6eV InGaAsSb DH TPV diodes grown also by OMVPE, where the bandgap is estimated from the external quantum efficiency (EQE) which is shown in Figure 10 The diodes that are presented in Figure 10 had fill factors of 68%,70%, and 72% for 0.5eV, 0.53eV, and 0.6eV respectively and the voltage factors ( $V_{\text{OC}}/E_{\text{G}}$ ) were nearly constant at 58% for  $\sim 2\text{A/cm}^2$  light generated current at  $T_{\text{diode}}=27^\circ\text{C}$ . The open circuit voltage and fill factor of the InGaAsSb TPV diodes



presented in this article do not significantly degrade as the InGaAsSb bandgap is reduced. This might be attributed to differences in growth conditions between the original work of reference [9] and recent TPV diodes. Because the InGaAsSb alloy begins to phase separate near 0.5eV, the material quality is dependent on the growth conditions, most importantly the growth temperature which must be optimized to minimize/prevent phase separation and the defects associated with them [9]. Figure 11 shows the measured diode dark current density and ideality factor vs. InGaAsSb bandgap of the same diodes presented in Figure 10. The average dark currents and standard deviations represent statistical data taken from batch-processed sets of 24, 24, and six 0.5cm<sup>2</sup> TPV diodes (the six diode batch corresponds to the larger error bars in the figure). The ideality factor is near unity for all bandgaps and the dark current density decreases proportionally to the square of the intrinsic carrier density which is proportional to  $\exp(-E_{\text{gap}}/kT)$ : these observations suggest that the material quality is nearly constant over this bandgap range.

### 8.0 In-cavity measurements of thermal-to-electric TPV conversion efficiency ( $\eta_{\text{TPV}}$ )

The performance of a TPV module using 0.5cm<sup>2</sup> P/N 0.53eV InGaAsSb DH TPV diodes has been measured in a prototypic test cavity, described in reference [3,4,25]. Thermal-to-electric efficiency in this test was measured as the ratio of peak module electric power to total module heat absorption rate. These parameters were measured simultaneously to assure validity of the final efficiency value. Modules were built with both a 1cm<sup>2</sup> (2 cells) and 4 cm<sup>2</sup> (8 cells) area. A front surface filter, with spectral efficiency calculated from reflection data to be  $\eta_{\text{Spectral}} \approx 79\%$ , is joined to both modules with epoxy. The photonic cavity is prototypical of a flat-plate TPV generator design, where the radiator is a large flat silicon carbide surface. The TPV module was fixed to the top of a copper pedestal to facilitate heat absorption measurements. The test was run in vacuum to eliminate conductive and convective heat transfer. The photonic cavity provides an optimal test environment for TPV efficiency measurements because it incorporates all known phenomena found in a practical operating TPV system, such as: non-ideal radiator emissivity, full radiator spectral and angular dispersion, photon recycling, and complex module geometry.

Table 1 gives the efficiency and output power parameters of 0.53eV InGaAsSb TPV diodes measured in-cavity, where the measured diode voltage and current represents an average value for each InGaAsSb TPV diode in the module. Both 1cm<sup>2</sup> and 4cm<sup>2</sup> diode modules were tested with equivalent results. The performance parameters are quoted for three different TPV diode temperatures which were approximately 30°C, 50°C, and 70°C. As predicted the open circuit voltage, power density, and efficiency

decrease rapidly with increasing temperature, and to a lesser extent the fill factor decreases also. Repeatable measurements yield a thermal-to-electric conversion efficiency of  $\eta_{\text{TPV}} \approx 19.7\%$  at a radiator temperature of  $950^\circ\text{C}$  and diode temperature of  $\sim 30^\circ\text{C}$  using  $0.53\text{eV}$  InGaAsSb TPV diodes with front surface spectral control filters. The semi-empirical TPV limit to the diodes used for this module is  $\eta_{\text{TPV}} = 26\%$  at  $0.75\text{W}/\text{cm}^2$  with absorbing substrates/back contacts and absolute intrinsic Auger limited performance is  $\eta_{\text{TPV}} = 30\%$  at  $0.85\text{W}/\text{cm}^2$ . At room temperature, the average  $0.53\text{eV}$  InGaAsSb TPV diode and efficiency is only 2/3 of the intrinsic Auger limited efficiency where the largest fraction of the difference being the limited experimental open circuit voltage.

**Table 1. Measured thermal-to-electric efficiencies for nominal  $0.53\text{eV}$  InGaAsSb TPV diode modules.**

TPV Diode Parameter	$T_{\text{diode}} \approx 30^\circ\text{C}$	$T_{\text{diode}} \approx 50^\circ\text{C}$	$T_{\text{diode}} \approx 70^\circ\text{C}$
$V_{\text{OC}}$ (volts)	0.306	0.273	0.247
$J_{\text{SC}}$ (amps/ $\text{cm}^2$ )	2.92	3	3
Module Fill Factor (%)	67	63	60
Power Density ( $\text{W}/\text{cm}^2$ )	0.6	0.52	0.45
Thermal to Electric Efficiency (%)	19.7	16.9	14.6

The primary factors attributed to the difference between measured  $0.53\text{eV}$  InGaAsSb TPV performance and the semi-empirical limits are:

- i. Spectral efficiency was calculated to be 79% based on reflection and transmission data, the semi-empirical limits assume 87%
- ii. The semi-empirical limit of  $\eta_{\text{TPV}} = 30\%$  at  $27^\circ\text{C}$  requires recombination to be dominated by intrinsic Auger recombination; the previous results and discussion section of Section 9.0 indicate that the open circuit voltage of the  $0.53\text{eV}$  InGaAsSb TPV diodes are limited by Shockley Read Hall defect recombination
- iii. The semi-empirical limits assume 90% active area, the measured module is 84% active area
- iv. The diodes in this module do not have a back surface reflector.

## 9.0 Discussion of InGaAsSb TPV diode modeling and experimental results

Semi-empirical limits to 0.53eV InGaAsSb TPV efficiency and power densities provide an upper limit to the thermal-to-electric conversion efficiency and power density of 0.53eV InGaAsSb TPV diodes of  $\eta_{\text{TPV}} \approx 30\%$  and  $\text{PD} \approx 0.85 \text{ W/cm}^2$  for  $T_{\text{radiator}} = 950^\circ\text{C}$  and  $T_{\text{diode}} = 27^\circ\text{C}$  compared to measured values of  $\eta_{\text{TPV}} \approx 20\%$  and  $\text{PD} \approx 0.60 \text{ W/cm}^2$ . The primary diode performance parameter responsible for this absolute difference,  $\Delta\eta_{\text{Total}} = [\eta_{\text{TPV}}(\text{semi-empirical limit}) - \eta_{\text{TPV}}(\text{measured})] \approx 10\%$ , is the open circuit voltage. The open circuit voltage of these devices reduces the actual measured efficiency from the semi-empirical limit by  $\Delta\eta_{\text{Voc}} \approx 4\text{-}5\%$  absolute. The fill factor, which is theoretically linked to open circuit voltage accounts for  $\eta_{\text{FF}} \approx 1.5\%$  absolute. Additional sources of discrepancy between the measured and semi-empirical limit to efficiency are differences between assumed and spectral efficiency used in the in-cavity testing ( $\eta_{\text{Spectral}} \approx 1.5\%$  absolute). Additional losses could be contributed to (i) less than unity internal quantum efficiency at short-wavelengths ( $< 1600\text{nm}$ ) and at the filter edge ( $\sim 2400\text{nm}$ ) and the (ii) additional inactive area in the measured TPV diode module compared to that assumed in the semi-empirical limit. Theoretically, the fill factor and open circuit voltage are both limited by the diode dark current, thus the carrier generation/recombination dynamics appear to be the primary limitation to 0.53eV InGaAsSb TPV diode performance. Sections 3-5 established theoretically the influence of material defects, interface recombination, and parasitic absorption on the diode's open circuit voltage and the requirements necessary to approach the semi-empirical Auger limited performance.

Carrier collection (Quantum efficiency) is not predicted to be a major source of loss in the thermal-to-electric conversion process for the carrier recombination coefficients and radiation spectrum ( $T_{\text{radiator}} = 950^\circ\text{C}$ ) assumed in this work. Measured internal quantum efficiencies (IQE) show peak IQEs of unity however the measured quantum efficiency decreases at wavelengths below 1600nm, the bandgap wavelength of the GaSb contact layer. The dominant loss mechanism in the quantum efficiency of 0.53eV InGaAsSb TPV diodes is in the absorption of short wavelength photons in this GaSb layer. We have shown experimentally that the short-wavelength IQE degradation can be alleviated by chemically thinning the GaSb cap and quantum efficiency simulations give good agreement with measurements for various cap thicknesses. The high bandgap of AlGaAsSb window layers, while successfully acting as a barrier to minority carriers generated within the active InGaAsSb layer, also prevents minority carrier diffusion into the active InGaAsSb layer from carriers generated in the GaSb contact layer. This further reduces the short wavelength quantum efficiency. However

simulations indicate that process/growth optimizations incorporating very thin GaSb caps (a few 10's of nanometer) will enable near unity quantum efficiency. In addition the authors of reference [22] indicated a small increases in quantum efficiency are possible with two-pass back surface reflector designs.

Unlike the quantum efficiency, the diode's open circuit voltage is predicted to sensitive to the values of the minority carrier recombination coefficients that were considered in these simulations. The semi-empirical limits predict that room temperature open circuit voltages of  $\sim 370\text{mV}$  can be obtained in  $0.53\text{eV}$  InGaAsSb diode architectures having back surface reflectors, negligible defect recombination, and the appropriate doping levels. We have found however that the actual measured open circuit voltage is constrained to approximately  $310\text{-}320\text{mV}$  for a number of various architectures, including a back surface reflector TPV diode. Experimental observations are summarized in the following list:

- The  $0.53\text{eV}$  InGaAsSb TPV diode's open circuit voltage, fill factor, and quantum efficiency is independent of the choice of the shallow-emitter-N/P or thick-emitter-P/N architecture. This indicates there is not an asymmetrical growth asymmetry influencing performance such as surface roughening in Te-doped layers. It also suggests the surface is effectively passivated in P/N diodes by AlGaAsSb windows, since shallow emitter N/P devices reduce dark current if the front surface is dominating dark current. The previous work of reference [8] discussed InGaAsSb diodes having thick n-type absorbers that show very poor performance, however not all the diodes investigated in this previous report had double heterostructure surface passivation.
- For P/N device architectures, a p-type AlGaAsSb passivating window produces a higher open circuit voltage (lower dark current) than for a p-type GaSb window. This gives good agreement with minority carrier lifetime measurements in double heterostructure lifetime samples that show a 3X decrease in effective surface recombination velocity when using p-type AlGaAsSb confinement. The dark current of P/N InGaAsSb TPV diodes having p-GaSb window layers appear to be limited by front surface recombination.
- For N/P devices use of p-GaSb or p-AlGaAsSb heterostructure confinement as the p-side back surface field (BSF) produces the same open circuit voltage and low dark current as the best P/N devices. Considering the previous observation, this result suggests that the p-AlGaAsSb prevents minority carrier electrons from diffusing across the thin p-GaSb contact layer to the

front surface of the P/N architectures, however p-AlGaAsSb does not significantly affect the number of interfacial defect states at the p-InGaAsSb/AlGaAsSb interface compared to p-InGaAsSb/GaSb.

- Switching from n-type AlGaAsSb or GaSb as confinement for either P/N or N/P TPV diodes does not affect the open circuit voltage for either P/N or shallow emitter N/P devices.
- The open circuit voltage was not observed to change when (i) P-type InGaAsSb/AlGaAsSb interface recombination velocity was reduced from  $\sim 10^3$  cm/s to  $10^2$  cm/s. This suggests that the best performing (high  $V_{oc}$ ) 0.53eV InGaAsSb TPV diodes are not limited by surface recombination at the p-AlGaAsSb/InGaAsSb interface.
- The open circuit voltage was not observed to change when a partial back surface reflector was incorporated into a 0.53eV InGaAsSb TPV device, indicating that the open circuit voltages of state-of-the-art 0.53eV InGaAsSb TPV diodes are not dominated by radiative recombination.
- The open circuit voltage did not degrade at high n-type and p-type doping levels which is the predicted if Auger recombination begins to dominate the diode dark current. No significant dependence of open circuit voltage on either n-side or p-side doping levels was observed.

Comparison of measured open circuit voltage vs. doping and simulation presented in Section 6.3 suggests that the measured open circuit voltage vs. p-type and n-type doping levels follow the behavior predicted for a TPV device limited by defect (Shockley-Read-Hall) recombination. The above bulleted list provides evidence that the state-of-the-art 0.53eV InGaAsSb TPV diodes are not limited by surface recombination velocity, Auger recombination, or radiative recombination. Thus the experimental open circuit voltage and TPV efficiency of 0.53eV InGaAsSb TPV diodes are most likely limited by defect recombination. While reference [15] reports a bulk Shockley Read Hall recombination lifetime of 1.3 $\mu$ s in p-type material by extrapolating to zero doping, direct measurements of carrier lifetime set a lower bound to the SRH lifetime of 500ns in p-type InGaAsSb. The experimental lower bound in n-type InGaAsSb is >100ns, however a better estimate for the actual value is not available, and preliminary investigation of the excitation dependence of carrier lifetime in n-type InGaAsSb is indicative of greater SRH activity than in p-type InGaAsSb. As reference to other III-V semiconductors, Shockley Read Hall lifetimes of 5-14 $\mu$ s [26,27] have been reported in GaAs solar photovoltaics, suggesting that there is more defect activity in InGaAsSb materials. High densities of anti-site defects in GaSb-based material are responsible for the high p-type background concentration

and most donor-dopant species have been reported to be also be associated with deep levels [28]. There is not however sufficient published defect spectroscopy and previous work on InGaAsSb opto-electronic devices to correlate the anti-site defects with diode dark current. Further work determining the defect structure in p-type and n-type InGaAsSb and the Shockley-Read-Hall lifetime in n-type tellurium doped InGaAsSb will provide additional feedback.

## 10.0 Summary

InGaAsSb TPV diode modules integrated with front surface filters have demonstrated over 19% thermal-to-electric efficiency and  $\sim 0.6\text{W}/\text{cm}^2$  power density for hot side temperatures of  $950^\circ\text{C}$  and diode temperatures of  $27^\circ\text{C}$ . Approaching the semi empirical limit of 30% conversion efficiency will require (i) aggressive processing techniques to achieve 87% spectral efficiency and a highly reflective back surface with negligible parasitic absorption (requiring GaSb substrate removal and BSR design) (ii) reduction of n-side and p-side InGaAsSb surface recombination velocities of  $\ll 300\text{cm/s}$  and material quality improvements to approach the intrinsic Auger limited open circuit voltage. Systematic investigations of state-of-the-art in  $0.53\text{eV}$  InGaAsSb TPV diode and comparison with theoretical simulations suggest that the diode open circuit voltage, thus efficiency, is limited by Shockley Read Hall recombination. Further insight could be gained with better understanding of the defect levels and densities in both the n-type and p-type InGaAsSb TPV material.

## 11.0 References

- [1] P.F. Baldasaro, J.E. Raynolds, G.W. Charache, D.M. Depoy, C.T. Ballinger, T. Donovan, and J.M. Borrego, "Thermodynamic analysis of thermophotovoltaic efficiency and power density tradeoffs", *J. Appl. Phys.*, vol. 89, pp. 3319-3327, (2001).
- [2] Timothy J. Coutts and James S. Ward, "Thermophotovoltaic and photovoltaic conversion at high-flux densities", *IEEE Trans. Elec. Dev.*, vol. 46, no. 10, pp. 2145-2153 (1999).
- [3] EJ Brown, PF Baldasaro, SR Burger, LR Danielson, DM Depoy, JM Dolatowski, PM Fourspring, GJ Nichols, WF Topper "The Status of Thermophotovoltaic Energy Conversion Technology at Lockheed Martin Corp.", Proceedings of the 2<sup>nd</sup> International Energy Conversion Engineering Conference, 16-19 August 2004, Providence Rhode Island.
- [4] B. Wernsman, R.R. Siergiej, S.D. Link, R.G. Mahorter, M.N. Palmisiano, R.J. Wehrer, R.W. Shultz, R.L. Messham, S. Murray, C.S. Murray, F. Newman, D. Taylor, D. Depoy, and T. Rahmlow, "Greater than 20% radiant heat conversion efficiency of a thermophotovoltaic radiator/module system using reflective spectral control" *IEEE Trans. Elec. Dev.*, vol. 51, no. 3, pp. 512-516, (2004).
- [5] T.D. Rahmlow, "Design Considerations and Fabrication Results for Front Surface TPV Spectral Control Filters", To be published Sixth Conference on Thermophotovoltaic Generation of Electricity, Freiburg, Germany 2004.

- [6] Patrick M. Fourspring and David M. DePoy, Thomas D. Rahmlow, Jr., Jeanne E. Lazo-Wasem, and Edward J. Gratrix, "Optical Coatings for Thermophotovoltaic Spectral Control," in Optical Interference Coatings on CD-ROM (The Optical Society of America, Washington, DC, 2004), ThE10.
- [7] G.W. Charache, P.F. Baldasaro, L.R. Danielson, D.M. Depoy, M.J. Freeman, C.A. Wang, H.K. Choi, D.Z. Garbuzov, R.U. Martinelli, V. Khalfin, S. Saroop, J.M. Borego, "InGaAsSb thermophotovoltaic diode: Physics Evaluation", *J. Appl. Phys.*, vol. 85, pp. 2247-2252, (1999).
- [8] C.W. Hitchcock, R.J. Gutmann, J.M. Borego, I.B. Bhat, G.W. Carache, "Antimonide-based devices for thermophotovoltaic applications" , *IEEE Trans. Electr. Devices*, vol. 46, no. 10, pp. 2154-2161 (1999).
- [9] C.A. Wang, H.K. Choi, S.L Ransom, G.W. Charache, L.R. Danielson, and D.M. Depoy, "High-quantum-efficiency GaInAsSb/GaSb thermophotovoltaic devices", *Appl. Phys. Lett.*, 75, pp. 1305-1307, (1999)
- [10] H.K. Choi, C.A. Wang, G.W. Turner, M.J. Manfra, D.L. Spears, G.W. Charache, L.R. Danielson, and D.M Depoy, " High performance GaInAsSb thermophotovoltaic devices with an AlGaAsSb window", *Appl. Phys. Lett.*, 71, pp. 3758-3760, (1997)
- [11] M.W. Dashiell, J.F. Beausang, G. Nichols, D.M. Depoy<sup>a</sup>, L.R. Danielson, H. Ehsani, K.D. Rahner, J. Azarkevich, P. Talamo, E. Brown, S. Burger, P. Fourspring, W. Topper, P.F. Baldasaro, C.A. Wang, R. Huang, M. Connors, G. Turner, Z. Shellenbarger, G. Taylor, Jizhong Li, R. Martinelli, D. Donetski, S. Anikeev, G. Belenky and S. Luryi, D.R. Taylor, J. Hazel "0.52 eV Quaternary InGaAsSb Thermophotovoltaic Diode Technology" , To be published Sixth Conference on Thermophotovoltaic Generation of Electricity, Freiburg, Germany 2004.
- [12]. S.M. Sze, "Physics of Semiconductor Devices", 2<sup>nd</sup> Edition, John Wiley and Sons, Inc. 1981.
- [13] W. Shockley and H.A. Queisser, "Detailed balance limit of efficiency of p-n junction solar cells", *J. Appl. Phys.*, vol. 32, pp. 510, (1961).
- [14] C. H. Henry, "Limiting efficiencies of ideal single and multiple energy gap terrestrial solar cells" *J. Appl. Phys.*, vol. 51, pp. 4494-4500, (1980).
- [15] S. Anikeev, D. Donetski, G. Belenki, S. Luryi, C.A. Wang, J.M. Borrego, G. Nichols, "Measurement of the Auger Recombination rate in p-type 0.54eV GaInAsSb by time-resolved photoluminescence", *Appl. Phys. Lett.*, vol. 83, pp. 3317-3319 (2003)
- [16] D. Donetski, , S. Anikeev, G. Belenky, S. Luryi, C.A. Wang, G. Nichols, " Reduction of interfacial recombination in GaInAsSb/GaSb double heterostructures", *Appl. Phys. Lett.*, 81, pp4769-4771 (2002)
- [17] D. Donetski, S. Anikeev, N. Gu, G. Belenky, S. Luryi, C.A. Wang, D.A. Shiao, M. Dashiell, J. Beausang, and G. Nichols, "Analysis of recombination processes in 0.5-0.6eV epitaxial GaInAsSb lattice matched to GaSb", To be published Sixth Conference on Thermophotovoltaic Generation of Electricity, Freiburg, Germany 2004.
- [18] W. van Roosbroeke and W. Shockley, "Photon-radiative recombination of electrons and holes in germanium", *Physical Review*, vol. 94, pp. 1558-1560, (1954).
- [19] P. Asbeck, "Self-absorption effects on the radiative lifetime in GaAs-GaAlAs double heterostructures", *J. Appl. Phys.*, vol. 48, pp. 820-822, (1977).
- [20] A. Marti, J.L. Balenzategui, R.F. Reyna, "Photon recycling and Schockley's diode equation", *J. Appl. Phys.*, vol. 82, no 8, pp. 4067-4075 (1997).
- [21] Martin A. Green, "Limits on the open-circuit voltage and efficiency of silicon solar cells imposed by intrinsic Auger processes", *IEEE Transactions on Electron Devices*, vol. ED-31, pp. 671-678, (1984)

- [22] R.K. Huang, C.A. Huang, M.K. Connors, G.W. Turner, "Hybrid Back Surface Reflector GaInAsSb Thermophotovoltaic Devices", To be published Sixth Conference on Thermophotovoltaic Generation of Electricity, Freiburg, Germany 2004
- [23] R. Huang, C.A. Wang, C.T. Harris, M.K. Connors, D.A. Shiau "Ohmic Contacts to n-type GaSb and n-type GaInAsSb", Accepted for Publication in Journal of Electronic Materials
- [24] S.J. Adachi, J. Appl. Phys., vol. 66, no. 12, pp. 6030-6040 (1989)
- [25] C.K. Gethers, C.T. Ballinger, and D.M DePoy, in Thermophotovoltaic Generation of Electricity - 4<sup>th</sup> NREL Conference Proceedings, Denver CO, 1998, p. 335-348, AIP Proceedings 460.
- [26] J.M. Olsen, R.K. Ahrenkiel, D.J. Dunlavy, B. Keyes, and A.E. Kibbler, "Ultralow recombination velocity at GaInP/GaAs Heterointerfaces" Applied Physics Letters, vol. 55, no. 12, pp. 1208-1210 (1989).
- [27] L.W. Molenkamp, G.L.M. Kampschoer, W. deLange, J.W.F.M Maes, and P.J. Roksnoer, "Ultralong minority-carrier lifetimes in GaAs grown by low-pressure organometallic vapor-phase epitaxy", Applied Physics Letters, vol. 54, no. 20, pp. 1992-1994 (1989).
- [28] A.G. Milnes and A.Y. Polyakov, "Review: Gallium Antimonide Device Related Properties", Solid-State-Electronics, vol. 36, no.6, pp. 803-818, (1993).
- [29] Expressions fit from mobility data of InGaAsSb layers grown on insulating GaAs substrates given in C.A. Wang, H.K. Choi, D.C. Oakley, G.W. Charache, J. Crystal Growth, vol 195, (1998) p. 346.



## Appendix

**Table AI. Spectral assumptions made in modeling for 0.53eV TPV**

Radiator temperature	950°C
Area	$A_1 = 1\text{cm}^2$ Total cell area $A_2 = 0.9\text{cm}^2$ Active cell area
Radiator emissivity	$\epsilon_{\text{rad}1} = 0.9$ above bandgap $\epsilon_{\text{rad}2} = 0.9$ below bandgap
TPV cell reflectivity	$R_1 = 0.97$ $< E_G$ , active area $R_2 = 0.15$ $> E_G$ , active area $R_3 = 0.97$ $< E_G$ , inactive area $R_4 = 0.97$ $> E_G$ , inactive area
Parasitic absorbance	$A_{\text{parasitic}} = 0.02$
Area weighted cell emissivity	$\epsilon_{\text{mod}1} = \frac{A_2}{A_1}(1 - R_2) + (1 - \frac{A_2}{A_1})(1 - R_4) : > E_G$ $\epsilon_{\text{mod}2} = \frac{A_2}{A_1}(1 - R_1) + (1 - \frac{A_2}{A_1})(1 - R_3) : < E_G$
Effective emissivity of radiator / cell combination	$\epsilon_{\text{eff}1} = \left( \frac{1}{\epsilon_{\text{rad}1}} + \frac{1}{\epsilon_{\text{mod}1}} - 1 \right)^{-1} : > E_G$ $\epsilon_{\text{eff}2} = \left( \frac{1}{\epsilon_{\text{rad}2}} + \frac{1}{\epsilon_{\text{mod}2}} - 1 \right)^{-1} : < E_G$
Total heat absorbed that can be converted to electricity	$P_1 = A_2 \int_0^{E_G} \frac{\epsilon_{\text{eff}1}}{\epsilon_{\text{mod}1}} \frac{2\pi E^3 dE}{h^3 c^2 (e^{E/kT} - 1)} (1 - R_2 - A_{\text{Parasitic}})$
Total heat absorbed	$P_2 = A_2 \int_0^{E_G} \frac{\epsilon_{\text{eff}1}}{\epsilon_{\text{mod}1}} \frac{2\pi E^3 dE}{h^3 c^2 (e^{E/kT} - 1)} (1 - R_2)$ $+ (A_1 - A_2) \int_{E_G}^{\infty} \frac{\epsilon_{\text{eff}1}}{\epsilon_{\text{mod}1}} \frac{2\pi E^3 dE}{h^3 c^2 (e^{E/kT} - 1)} (1 - R_4)$ $+ A_2 \int_0^{E_G} \frac{\epsilon_{\text{eff}2}}{\epsilon_{\text{mod}2}} \frac{2\pi E^3 dE}{h^3 c^2 (e^{E/kT} - 1)} (1 - R_1)$ $+ (A_1 - A_2) \int_0^{E_G} \frac{\epsilon_{\text{eff}2}}{\epsilon_{\text{mod}2}} \frac{2\pi E^3 dE}{h^3 c^2 (e^{E/kT} - 1)} (1 - R_3)$
Spectral efficiency	$\eta_{\text{spectral}} = \frac{A_2 \int_0^{E_G} \frac{\epsilon_{\text{eff}1}}{\epsilon_{\text{mod}1}} \frac{2\pi E^3}{h^3 c^2 (e^{E/kT} - 1)} (1 - R_2 - A_{\text{Parasitic}}) dE}{A_1 \int_0^{E_G} \frac{\epsilon_{\text{eff}2}}{\epsilon_{\text{mod}2}} \frac{2\pi E^3}{h^3 c^2 (e^{E/kT} - 1)} dE + A_1 \int_{E_G}^{\infty} \frac{\epsilon_{\text{eff}1}}{\epsilon_{\text{mod}1}} \frac{2\pi E^3}{h^3 c^2 (e^{E/kT} - 1)} dE} = 87\%$
TPV efficiency	$\eta_{\text{TPV}} = \frac{V_{OC} \times I_{SC} \times FF}{P_1} \times \eta_{\text{spectral}} = \eta_{\text{Diode}} \times \eta_{\text{spectral}}$

**Table AII. 0.53eV InGaAsSb device parameters used in simulations**

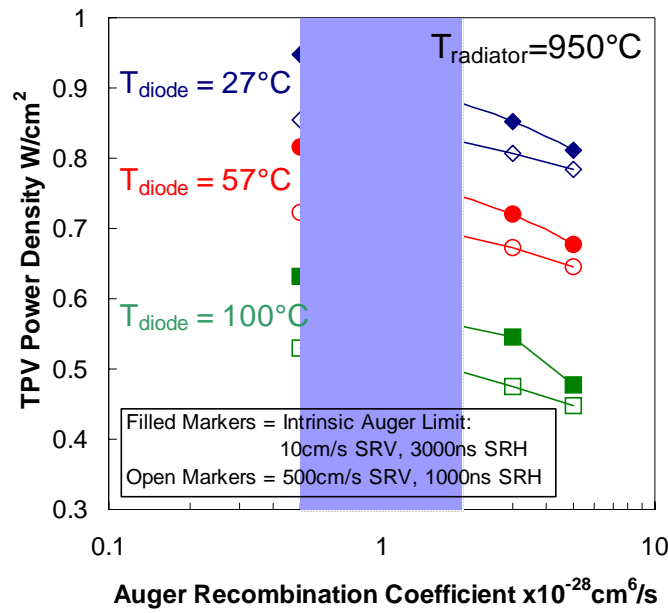
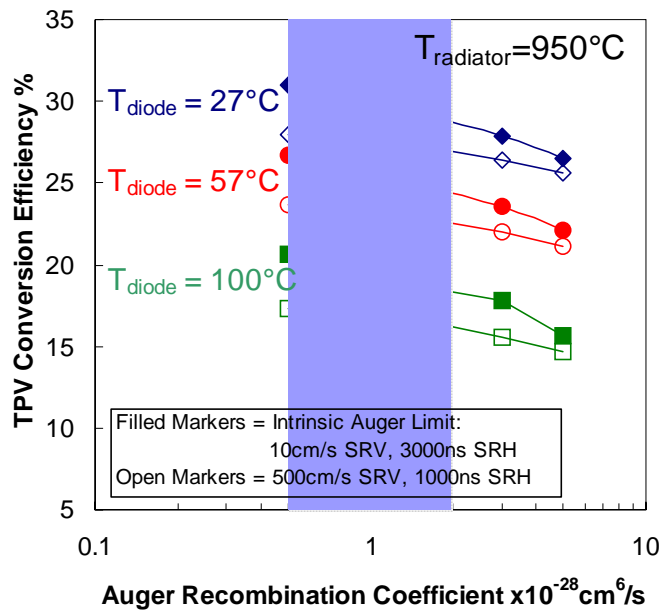
$T_{\text{Diode}} / E_G$	$T = 300\text{K} / E_G = 0.53\text{eV}$
Density of states	$N_C = 1.5 \times 10^{17} \text{cm}^{-3}, N_V = 7 \times 10^{18} \text{cm}^{-3}$ [24]
Intrinsic electron density	$n_i^2 = N_C N_V \exp\left(-\frac{E_G}{kT_{300\text{K}}}\right) = 4.5 \times 10^{13} \text{cm}^{-3}$
Refractive index	$n = 3.45$
Absorption coefficient	$\alpha(E) = A_o (E - E_G)^{0.5}$ where $A_o = 2.6 \mu\text{m}^{-1} \text{eV}^{-0.5}$
Radiative recombination coefficient [18]	$B = \frac{1}{n_i^2} \int_{\theta=0}^{\theta=\pi} \int_{\phi=0}^{\phi=2\pi} \int_{E=0}^{E=\infty} n^2 \alpha(E) \frac{\partial \Gamma(E)}{\partial E \partial \phi \partial \theta} \sin \theta dE d\phi d\theta \quad (\text{cm}^3 \cdot \text{s}^{-1})$ <p>where <math>\frac{\partial \Gamma(E)}{\partial E \partial \phi \partial \theta} = \frac{2E^2}{h^3 c^2} \left( \exp\left(\frac{E}{kT}\right) - 1 \right)^{-1} \quad (\text{cm}^2 \cdot \text{s} \cdot \text{eV} \cdot \text{sr})^{-1}</math></p>
	$B \approx 1 \times 10^{-10} \text{cm}^3/\text{s}$
Transmission coefficient for recombination photons internal to diode (forward direction) [19,20]	$T_{\text{back}}^{\text{forward}}(\theta, E) = \frac{(1 - R_{\text{back}}) R_{\text{front}} \exp\left[\frac{-(z+W)\alpha}{\cos \theta}\right]}{\left(1 - R_{\text{front}} R_{\text{back}} \exp\left[\frac{-2\alpha W}{\cos \theta}\right]\right)}$ $T_{\text{front}}^{\text{forward}}(\theta, E) = (1 - R_{\text{front}}) \exp\left[\frac{-z\alpha}{\cos \theta}\right] \frac{R_{\text{front}} R_{\text{back}} \exp\left[\frac{-2\alpha W}{\cos \theta}\right]}{\left(1 - R_{\text{front}} R_{\text{back}} \exp\left[\frac{-2\alpha W}{\cos \theta}\right]\right)}$
Photon recycling factor [19,20]	$\Phi^{-1} = \frac{\sum_i \int_{z=0}^{z=W} \int_{\theta=0}^{\theta=\pi} \int_{\phi=0}^{\phi=2\pi} \int_{E=0}^{E=\infty} n^2 \alpha(E) \frac{\partial \Gamma(E)}{\partial E \partial \phi \partial \theta} T_i(\theta, E) \sin \theta dE d\phi d\theta dz}{\int_{z=0}^{z=W} \int_{\theta=0}^{\theta=\pi} \int_{\phi=0}^{\phi=2\pi} \int_{E=0}^{E=\infty} n^2 \alpha(E) \frac{\partial \Gamma(E)}{\partial E \partial \phi \partial \theta} \sin \theta dE d\phi d\theta dz} \quad (\text{cm}^3 \cdot \text{s}^{-1})$
	integrate the term in the numerator for both front and back surfaces and for photons originating in both the forward and reverse directions
	$\Phi_{\text{Rback}=100\%} \approx 40, \Phi_{\text{Rback}=0\%} \approx 4$
Auger coefficient	$C_n = C_p = 1 \times 10^{-28} \text{cm}^6/\text{s}$ unless otherwise indicated
SRH Lifetime	Assume $\tau_{\text{SRH}} = 0.5$ to $1 \mu\text{s}$ for electrons and holes
SRV	$S_n = S_p$ varied from $10 \text{cm/s}$ to $2000 \text{cm/s}$ [14,15]
Electron and hole mobility model [29]	$\mu_e = 420 \frac{\text{cm}^2}{\text{V} \cdot \text{s}} + \frac{8500}{1 + \left(\frac{N_D}{5 \times 10^{17} \text{cm}^{-3}}\right)^{0.7}} \quad \mu_h = 110 \frac{\text{cm}^2}{\text{V} \cdot \text{s}} + \frac{500}{1 + \left(\frac{N_A}{9 \times 10^{17} \text{cm}^{-3}}\right)^{0.66}}$
Free carrier absorption in active region	Assumed to be negligible

## List of Figures

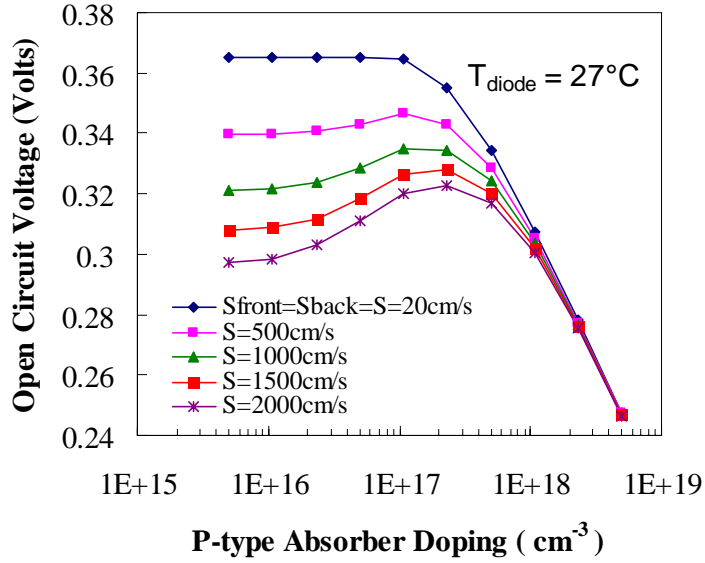
- Figure 1. Cross sectional schematic of 0.53eV N/P and P/N InGaAsSb TPV diode architectures.
- Figure 2. The semi-empirical efficiency (a) and power density (b) limits for  $T_{\text{radiator}}=950^{\circ}\text{C}$  of  $\sim 0.53\text{eV}$  InGaAsSb TPV diodes for three different TPV diode temperatures, plotted as a function of Auger recombination coefficient. The predictions assume the diode has a back surface reflector and (i) negligible bulk and interface recombination (solid markers) and also show the influence of (ii) non-negligible material/defect recombination (open markers).
- Figure 3 (a) Simulated open circuit voltage for a two-pass photon recycled TPV architecture having a back surface reflector (b) Simulated open circuit voltage for a single pass architecture (absorbing substrate/back contact). In the simulations the SRV and SRH-lifetime are assumed to be equal for both n-side and p-side.
- Figure 4. Internal quantum efficiency for 0.53eV N/P and P/N double heterostructure InGaAsSb TPV diodes.
- Figure 5. Measured internal quantum efficiency (markers) for 0.53eV N/P InGaAsSb TPV diode grown with a thick GaSb contact layer before and after chemically etching  $\sim 300\text{nm}$  of the GaSb. Simulations are shown for 550nm GaSb, 250nm, and 10nm thick GaSb (lines).
- Figure 6. Measured internal quantum efficiency of 0.53eV N/P InGaAsSb TPV diode with equivalent GaSb contact layer thicknesses having thin AlGaAsSb (triangles) and thin GaSb (squares) window layers. The inset shows the schematic energy band diagrams of the n-type GaSb contact layer, the window layer, and the emitter for each architecture.
- Figure 7. Plot of measured  $V_{\text{OC}}$  vs.  $J_{\text{SC}}$  data (markers) for various light-illuminations for 0.53eV P/N and N/P InGaAsSb TPV diodes. The inset provides information on whether GaSb or AlGaAsSb was used for the passivating window and back surface field. Simulations are shown as lines in the figure and are described in the text and the figure legend.
- Figure 8. Open circuit voltage (normalized to the diode band gap) vs. acceptor (zinc) doping in the thick p-type absorbing region for nominal 0.53eV InGaAsSb TPV diodes. Included also is a Hybrid back surface reflector device reported in [21].
- Figure 9. Open circuit voltage (normalized to the diode band gap) vs. donor (tellurium) doping in the thin n-type region for nominal 0.53eV InGaAsSb TPV diodes .
- Figure 10. Measured external quantum efficiency curves for 0.5, 0.53 and 0.6eV InGaAsSb TPV diodes.

Figure 11. Fitted values of dark current density and ideality factor vs. bandgap from measured illuminated current-voltage characteristics.

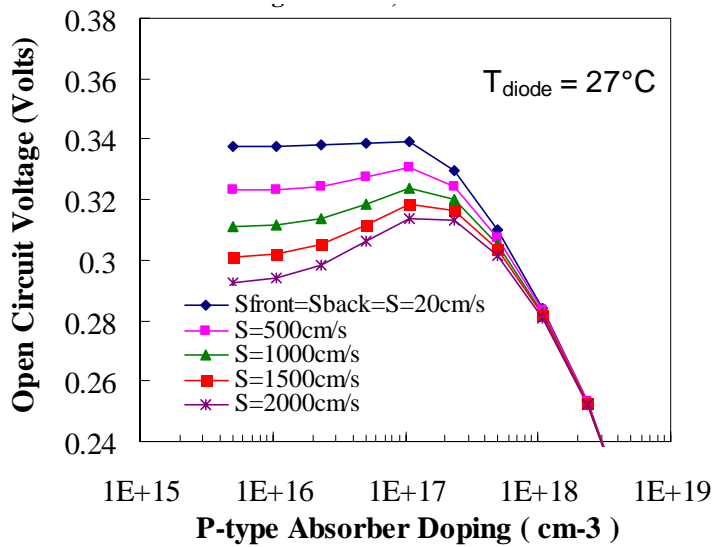




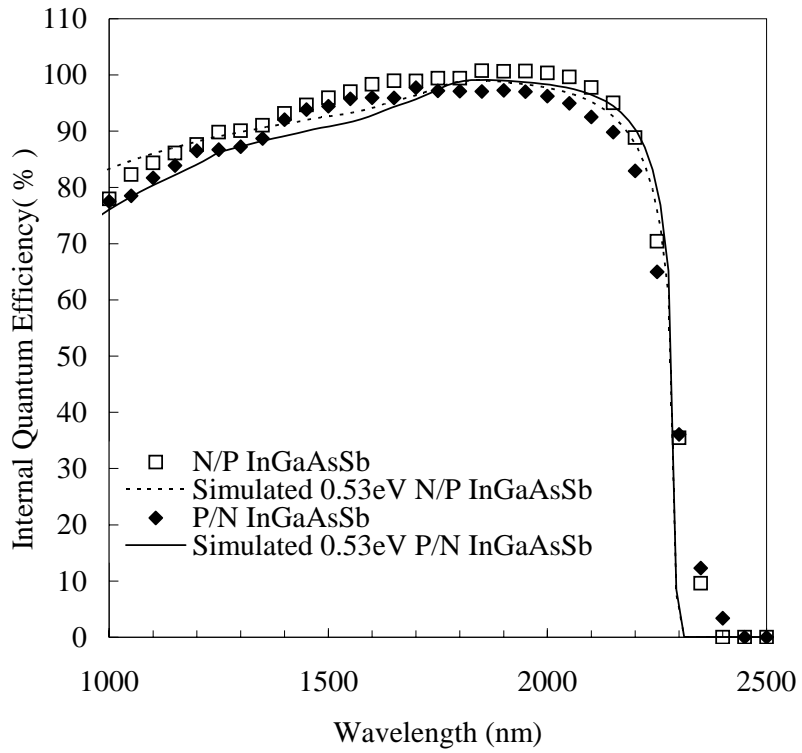
IEEE TED Figure 2 Dashiell et al.



IEEE TED Figure 3a Dashiell et al

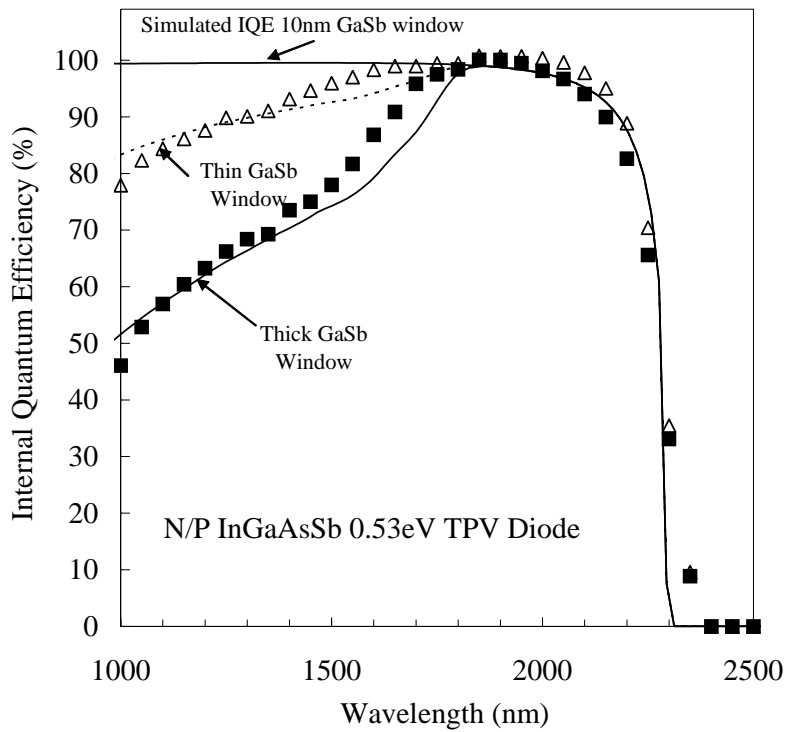


IEEE TED Figure 3b Dashiell et al.

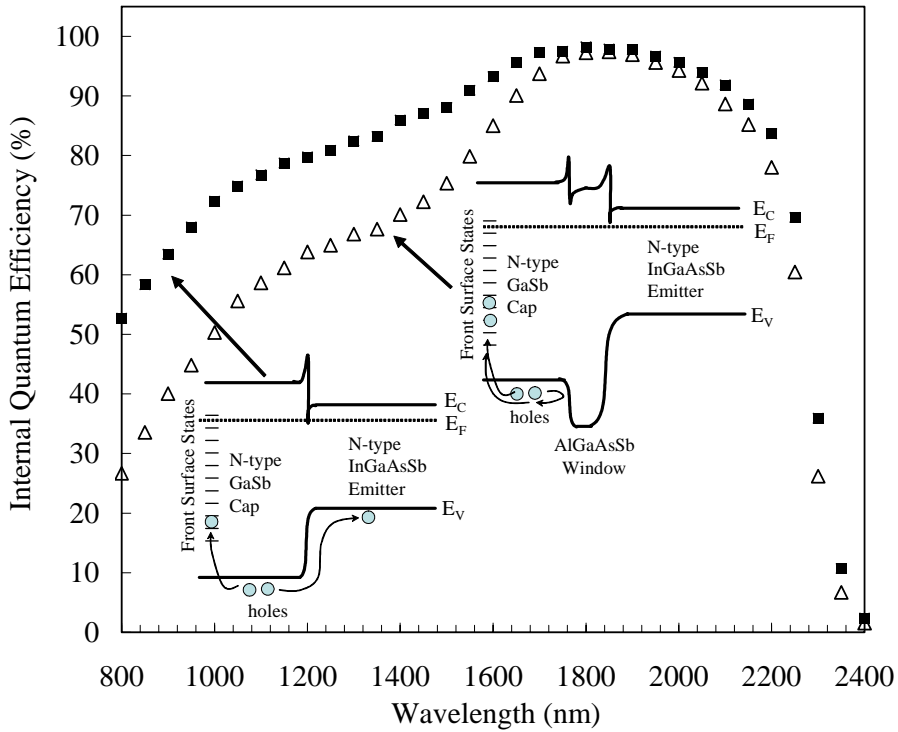


IEEE TED Figure 4 Dashiell et al.

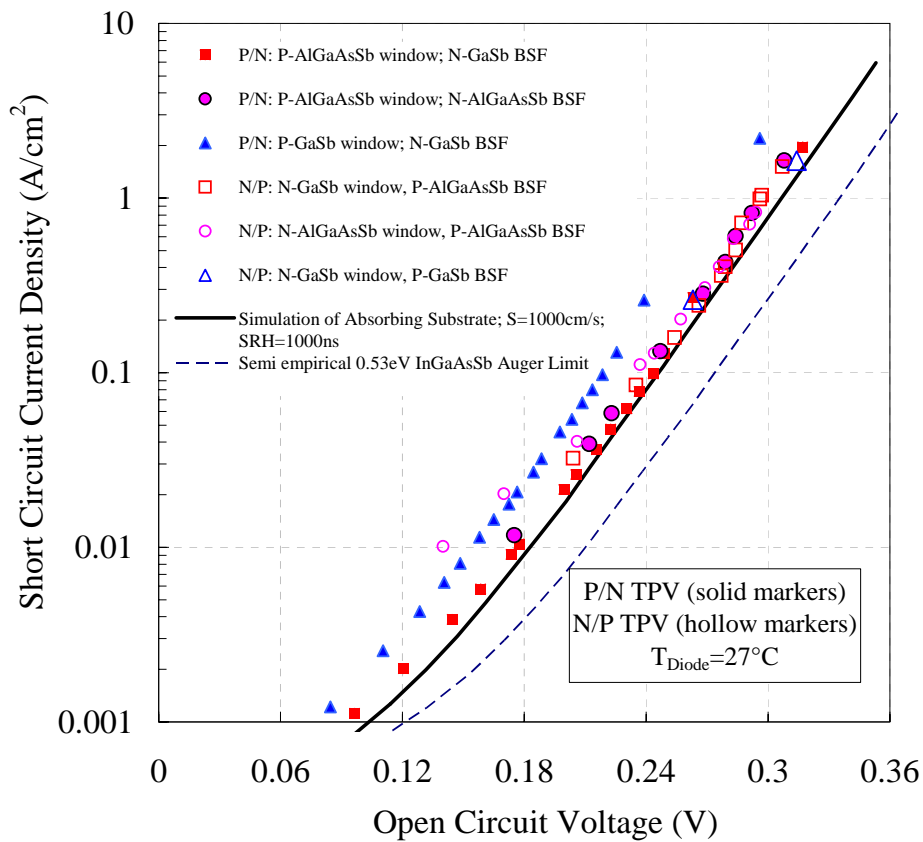




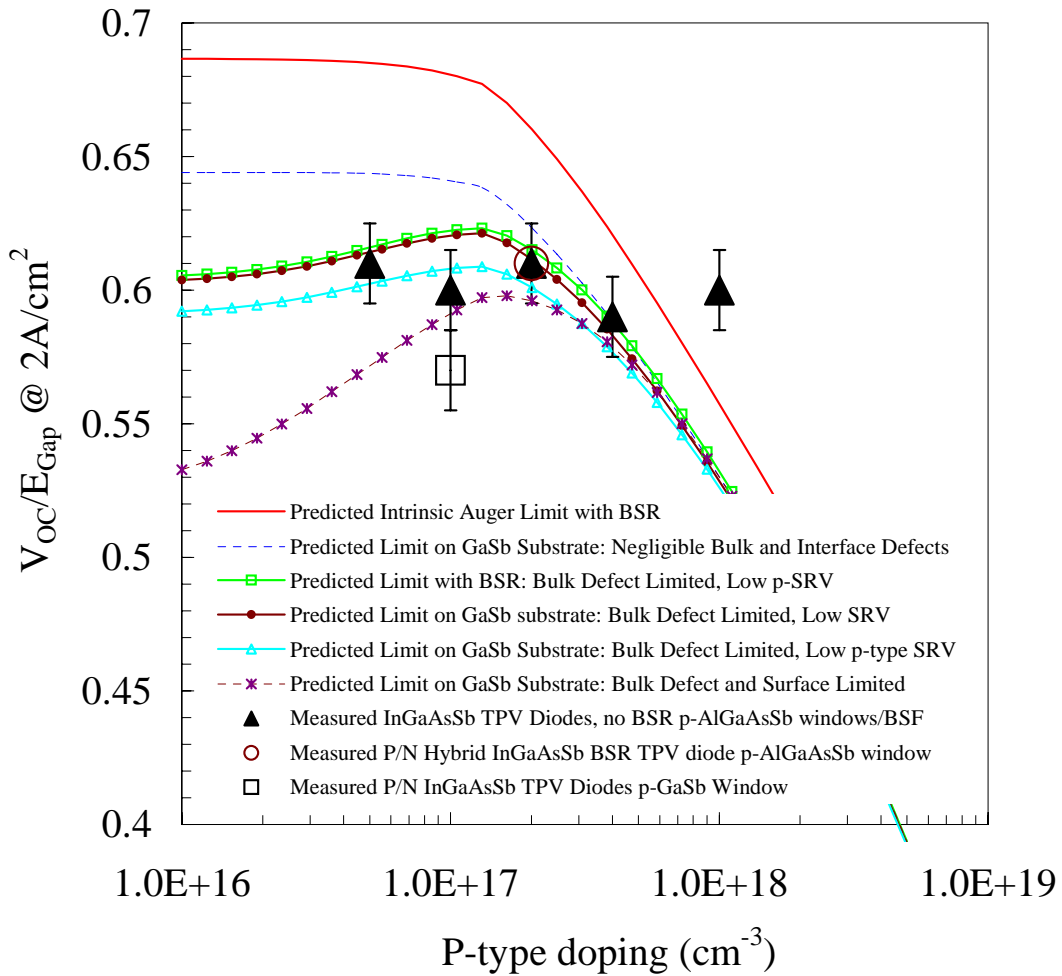
IEEE TED Figure 5 Dashiell et al.



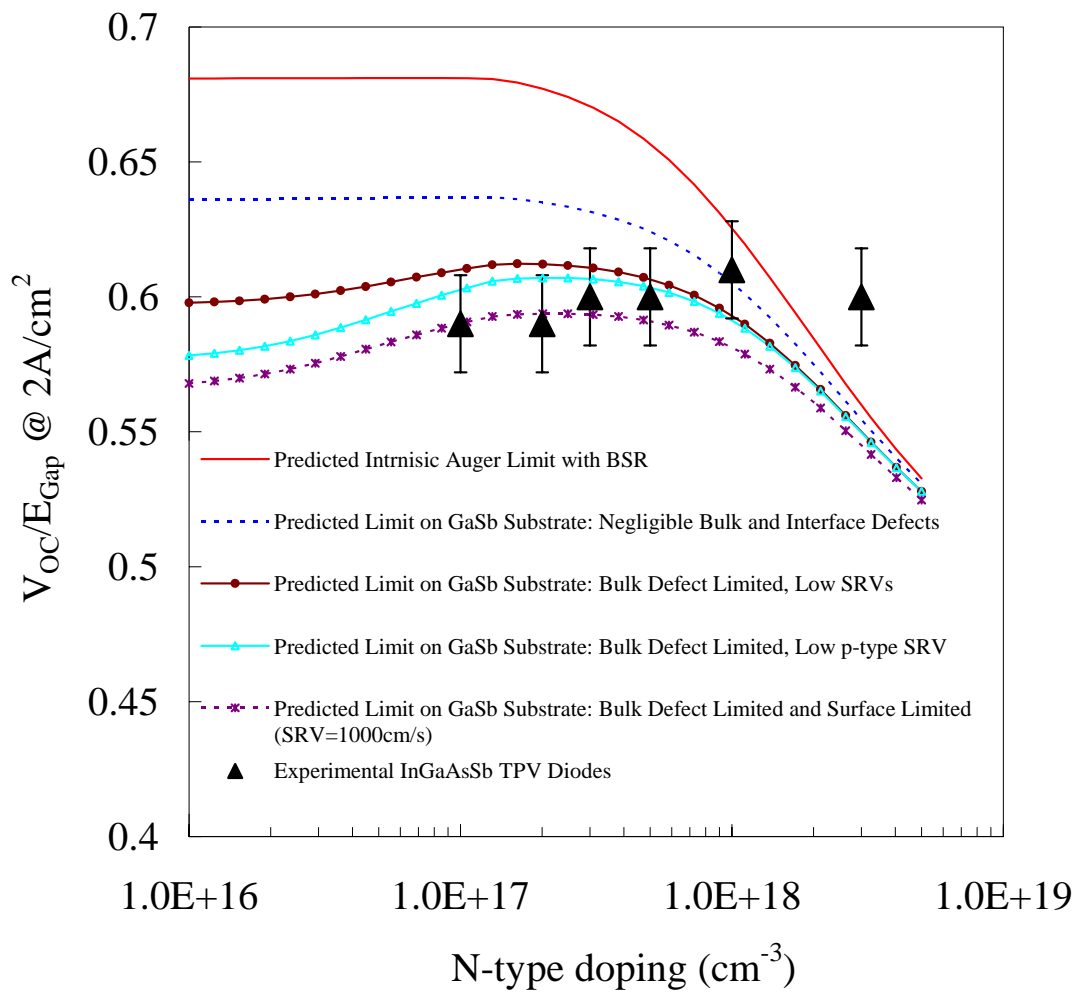
IEEE TED Figure 6 Dashiell et al.



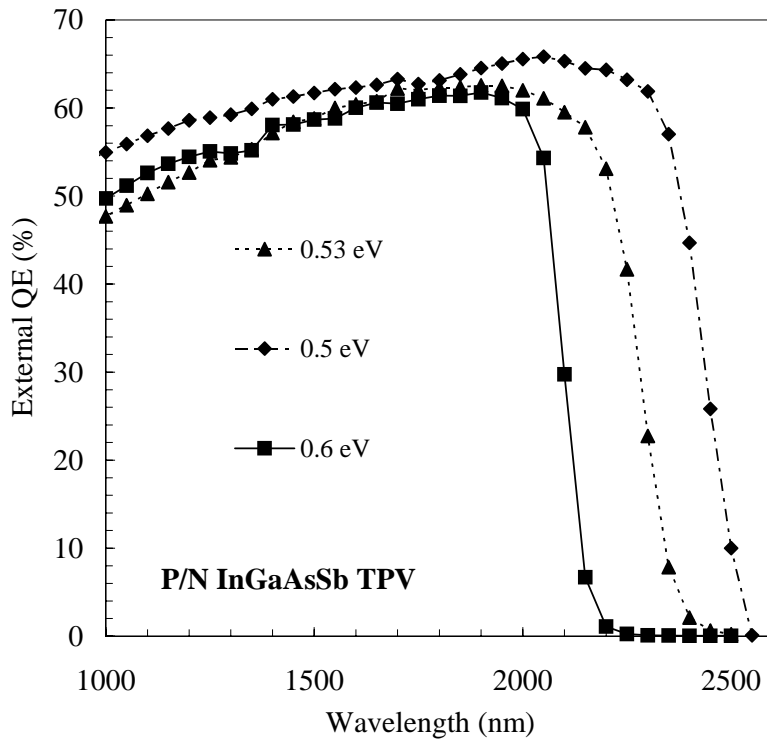
IEEE TED Figure 7 Dashiell et al.



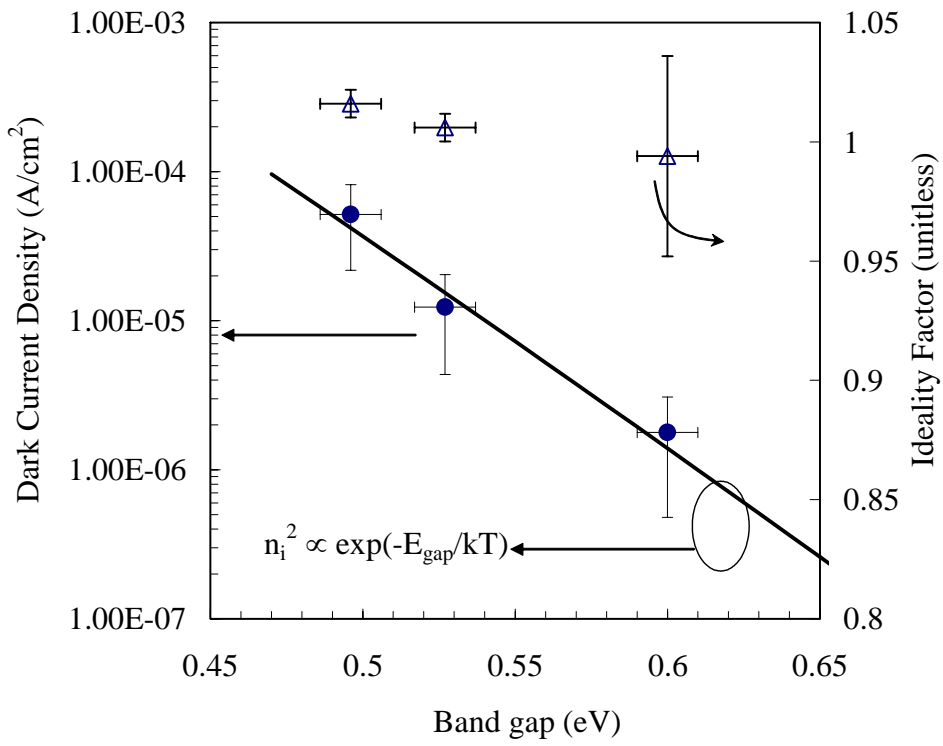
IEEE TED Figure 8 Dashiell et al.



IEEE TED Figure 9 Dashiell et al.



IEEE TED Figure 10 Dashiell et al.



IEEE TED Figure 11 Dashiell et al.